PROCEEDINGS of the
23rd International Congress on Acoustics
9 to 13 September 2019 in Aachen, Germany

Prediction of acoustic response on tube-rows with bias-flow using linearized Navier-Stokes equations in frequency domain

Wei NA[(1)], Susann BOIJ[(2)], Aswathy SURENDRAN[(3)], Dong YANG[(4)], Aimee MORGANS[(5)]

[(1,2)]KTH Royal Institute of Technology, Department of Aeronautical and Vehicle Engineering, Stockholm, Sweden, wein@kth.se
[(1,2)]KTH Royal Institute of Technology, The Marcus Wallenberg Laboratory for Sound and Vibration Research (MWL), Sweden
[(3,4,5)]Imperial College London, Department of Mechanical Engineering, UK, a.surendran@imperial.ac.uk

Abstract

Heat exchangers are widely used in industries where heat needs to be transferred from one fluid to another fluid. For example, there are plate-fin heat exchangers in gas turbine engines, shell and tube heat exchangers in oil refineries and tube bundle heat exchangers in domestic boilers. Among the different types of exchangers, tube bundle exchangers are the most commonly used heat exchange equipments. In this paper, heat exchanger with the structure of tube rows with bias flow and possible acoustic interaction at the tube row is studied for the acoustic reflection and transmission. The numerical methodology solving the linearized Navier-Stokes equation in the frequency domain is used. It has the advantage of taking into account the flow effects, viscous losses as well as thermal losses in the acoustic propagation. The simplified geometry for the heat exchanger investigated in this paper is a two-dimensional rectangular duct with two half cylinders with a bias flow going through the gap between the cylinders. In the current study, the acoustic response is predicted numerically with the cold flow only and compared to the experimental data, as a preparation for the next study with the hot flow.

Keywords: Heat Exchangers, Bias-flow, LNSE, Frequency domain

1 INTRODUCTION

Tube-rows exist widely in engineering applications, for example, in tube bundle heat exchangers, in domestic boilers, in air coolers. Multiple physical phenomenon can happen when flow passing through the tube rows. As addressed in [1], from the acoustic point of view, acoustic waves can scatter on the tube rows, leading to the sound transmission and reflection; flow separation due to the cross-flow, leading to the generation of the vorticity waves, etc.

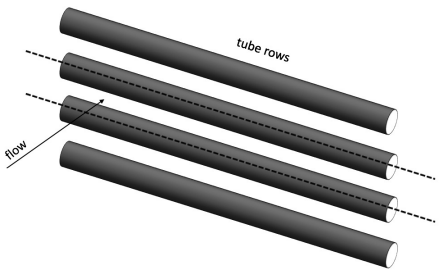

Figure 1. Schematic of three-dimensional tube-rows with bias-flow.

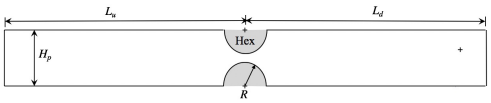

Figure 2. The simplified two-dimensional numerical geometry of the tube-row heat exchangers investigated in the paper, where $R = 10\,\text{mm}$, H_p=25 mm, $L_u = 40R$ and $L_d = 40R$, respectively.

An array of cylinders in cross-flow can be modelled as a single cylinder in a hard-walled flow-duct through

using the image sources method [1]. Therefore, the three-dimensional heat exchanger with tube-rows as Fig. (1) shown is simplified to the two-dimensional rectangular duct with two half cylinders as Fig. (2) illustrates. In the paper, the acoustic response is investigated numerically with the geometry as Fig. (2) shown with bias-flow at different Mach numbers.

When the flow is passing through the two half cylinders within the duct, a jet flow is formed. Recirculation zones are formed as well by shear layers along the jet flow. Such shear layers are unstable to low frequency perturbations, energy is transferred from the acoustic waves to the vorticity waves. It is of interest to investigate the flow-acoustic interaction for the tube-row heat exchangers.

2 NUMERICAL METHODOLOGY

The linearized Navier-Stokes equations are derived from the full compressible Navier–Stokes equations. A frequency domain approach has been taken by prescribing harmonic time-dependence of the perturbed quantities. In this way, any perturbed quantity can be represented as $q'(x,\omega,t) = \mathrm{Re}\{\hat{q}(x)e^{\mathrm{i}\omega t}\}$, where $\hat{q}$ is a complex quantity and ω is the angular frequency. The frequency domain linearized Navier-Stokes equations used in the paper are presented as:

$$\begin{aligned} \mathrm{i}\omega\hat{\rho} + \nabla\cdot(\rho_0\hat{\boldsymbol{u}} + \hat{\rho}\boldsymbol{u}_0) &= 0 \\ \mathrm{i}\omega\rho_0\hat{\boldsymbol{u}} + (\hat{\boldsymbol{u}}\cdot\nabla)\boldsymbol{u}_0 + (\boldsymbol{u}_0\cdot\nabla)\hat{\boldsymbol{u}} + \hat{\rho}(\boldsymbol{u}_0\cdot\nabla)\boldsymbol{u}_0 &= \nabla\cdot\boldsymbol{\sigma} \\ \rho_0 C_p(\mathrm{i}\omega\hat{T} + \hat{\boldsymbol{u}}\cdot\nabla T_0 + \boldsymbol{u}_0\cdot\nabla\hat{T}) + \hat{\rho}C_p(\boldsymbol{u}_0\cdot\nabla T_0) - (\mathrm{i}\omega\hat{p} + \hat{\boldsymbol{u}}\cdot\nabla p_0 + \boldsymbol{u}_0\cdot\nabla\hat{p}) - \frac{\hat{T}}{T_0}(\boldsymbol{u}_0\cdot\nabla p_0) &= \nabla\cdot(k\nabla\hat{T}) + \Phi \end{aligned} \tag{1}$$

with

$$\boldsymbol{\sigma} = -\hat{\boldsymbol{p}}\mathbf{I} + \mu(\nabla\hat{\boldsymbol{u}} + (\nabla\hat{\boldsymbol{u}})^T) + (\mu_B - \frac{2}{3}\mu)(\nabla\cdot\hat{\boldsymbol{u}})\mathbf{I}$$

and

$$\hat{\rho} = \rho_0(\frac{\hat{p}}{p_0} - \frac{\hat{T}}{T_0})$$

where a hat ˆ indicates a perturbed quantity, a subscript zero indicates mean flow quantities, ρ is the density, p is the pressure, $\boldsymbol{u}$ is the velocity vector, T is the temperature, ω is the angular frequency, μ is the dynamic viscosity. μ_B is the bulk viscosity, C_p is the heat capacities for constant pressure, k is the thermal conductivity, $\mathbf{I}$ is the unit matrix and Φ is the viscous dissipation of mechanical energy due to the shear viscosity and the fluid relaxation losses, which is a function of velocity, dynamic viscosity, and bulk viscosity, defined as:

$$\Phi = [\mu(\nabla\hat{\boldsymbol{u}} + (\nabla\hat{\boldsymbol{u}})^T) + (\mu_B - \frac{2}{3}\mu)(\nabla\cdot\hat{\boldsymbol{u}})\mathbf{I}]\cdot\nabla\hat{\boldsymbol{u}}$$

Boundary conditions are needed for each dependent variable. Different boundary conditions are set up for the top and the bottom duct walls as well as the walls of the heat exchangers. The following boundary conditions are used in simulations.

At the top and bottom duct walls, a rigid, symmetrical, adiabatic wall boundary condition is imposed as:

$$\hat{\boldsymbol{n}}\cdot\hat{\boldsymbol{u}} = 0, \quad \hat{\boldsymbol{n}}\cdot\nabla\hat{\rho} = 0 \quad \text{and} \quad -\hat{\boldsymbol{n}}\cdot(k\nabla\hat{T}) = 0 \tag{2}$$

In the vicinity of the heat exchangers, at the wall of two half cylinders, rigid, no-slip, isothermal wall boundary conditions are applied as:

$$\hat{\boldsymbol{u}} = 0, \quad \hat{\boldsymbol{n}}\cdot\nabla\hat{\rho} = 0 \quad \text{and} \quad \hat{T} = 0 \tag{3}$$

where $\hat{\boldsymbol{n}}$ is the unit vector normal to the duct wall. It should be noted that as the velocity components are restricted to zero on all edges.

3 BACKGROUND MEANFLOW

Linearization of the Navier–Stokes equations is performed by splitting the quantities of the total field into the mean part and the perturbed part, where the mean flow field is supposed to be obtained first for the following acoustic simulations. In this paper, the steady state mean flow is simulated with a compressible Reynolds-Averaged Navier–Stokes (RANS) solver, with the SST turbulence model. Figure (3) presents the steady state mean flow field of a simplified two-dimensional heat exchanger geometry when inlet flow speed is $\mathbf{u}_{in} = 11.5\,\mathrm{m/s}$, yielding a Mach number of $Ma = 0.033$. In the computational dynamic fluid (CFD) simulations, the velocity is prescribed at the inlet of the duct; the top and bottom of duct wall, the symmetric boundary condition is applied; on the two half cylinders, the non-slip wall boundary condition is applied together with the wall functions at $y^+ \approx 1$; at the outlet of the duct, an ambient pressure boundary condition is applied.

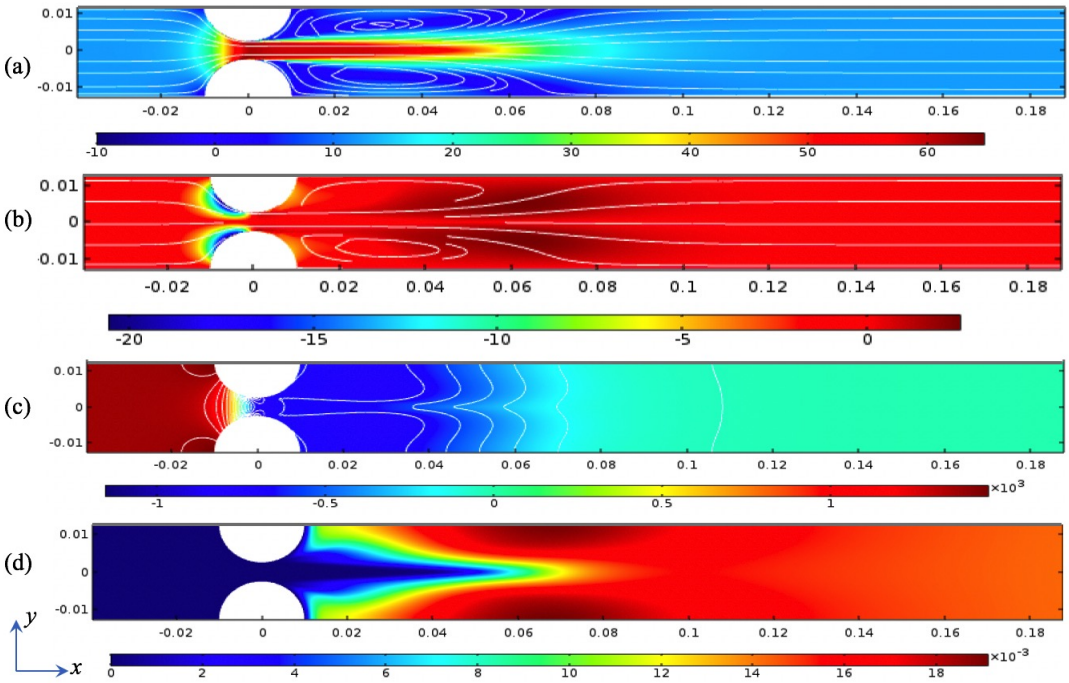

Figure 3. Mean flow field with the inlet flow speed $\mathbf{u}_{in} = 11.5\,\mathrm{m/s}$, yielding $Ma = 0.033$: (a) shows the flow velocity component u_{0x} and streamlines of the steady-state meanflow in [m/s]; (b) shows the flow velocity component u_{0y} in [m/s]; (c) shows the pressure p_0 in [Pa] and (d) shows the turbulent eddy viscosity μ_T in [Pa·s].

It is observed in Fig. (3) that a jet with a maximum flow speed of about $60\,\mathrm{m/s}$, i.e. $Ma \approx 0.175$ is formed downstream of the two half cylinders due to the geometrical contraction. The jet has a length of about 2–4 duct diameters, expanding into a channel flow, a recirculation zone thus exhibits. In the recirculation zone, the flow reattaches at about 3-5 duct diameters downstream of the two half cylinders. Further downstream, the flow is again the unperturbed channel flow. The sound–vortex interaction is assumed to happen at the shear layer of the jet flow.

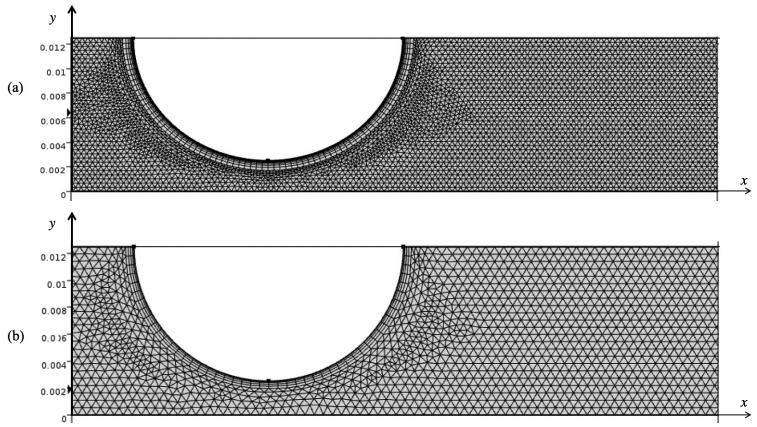

Figure 4. Schematic of the CFD mesh and the acoustic mesh in the vicinity of the half cylinder: (a) CFD mesh; (b) acoustic mesh.

4 MAPPING BETWEEN CFD AND ACOUSTICS MESH

In most numerical cases, the CFD mesh and the acoustic mesh are two independent meshes. The CFD mesh needs to be generated with respect of the characteristics of the flow field, while, the acoustic mesh can be generated with the rule of thumb that, 7 numerical cells per wave length are enough. In addition, the boundary layer mesh in the CFD mesh and in the acoustic mesh does not need the same resolution. For example, in the CFD simulations, in the near wall region, the flow boundary layer mesh is generated under the consideration of the dimensionless wall distance y^+ with 7-8 cells, however, the acoustic boundary layer mesh is generated within 4-5 cells, the thickness is frequency dependent and calculated by $\delta_A = \sqrt{(2\mu)/(\omega\rho)}$, where ρ is density of the fluid, μ is the dynamic viscosity and ω is the angular frequency.

When the CFD and the acoustic models are not solved on the same computational mesh, numerical noise can happen as the terms containing gradients of the background mean flow variables can become very noisy. Therefore, careful mapping of the CFD solution from the CFD mesh onto the acoustics mesh should be done in order not to introduce non-physical numerical noise into the acoustics solution. In the heat exchanger simulations, two different mesh are used as Fig. (4) shows. The acoustic mesh used for the solutions of the perturbed quantities is triangular mesh with about 54000 elements.

A mapping technique with mapping equations that smooths the background flow variables is used. In the mapping, the mean background flow pressure p_0, velocity field $\mathbf{u}_0$ and turbulent viscosity μ_T variables are mapped onto the corresponding variables on the acoustics mesh $p_{0(aco)}$, $\mathbf{u}_{0(aco)}$, and $\mu_{T(aco)}$. The mapping and smoothing is achieved by solving the Eq. (4):

$$\begin{aligned} p_{0(aco)} - p_0 &= \delta h^2 \nabla \cdot \nabla p_{0(aco)} \\ \mathbf{u}_{0(aco)} - \mathbf{u}_0 &= \delta h^2 \nabla \cdot \nabla \mathbf{u}_{0(aco)} \\ \mu_{T(aco)} - \mu_T &= \delta h^2 \nabla \cdot \nabla \mu_{T(aco)} \end{aligned} \tag{4}$$

where the term on the right hand side adds smoothing using isotropic diffusion. The amount of diffusion is controlled by the parameter δ (a constant that can be tuned) and the mesh size squared, h^2. The term in some sense corresponds to source term stabilization as known from CFD.

The comparison of the velocity profile between the CFD mesh and the acoustic mesh with mapping technique is plotted in Fig. (5). The mapping technique generally works well, there are only discrepancies at the sharp edge of the velocity profile, as Fig. (5) shown.

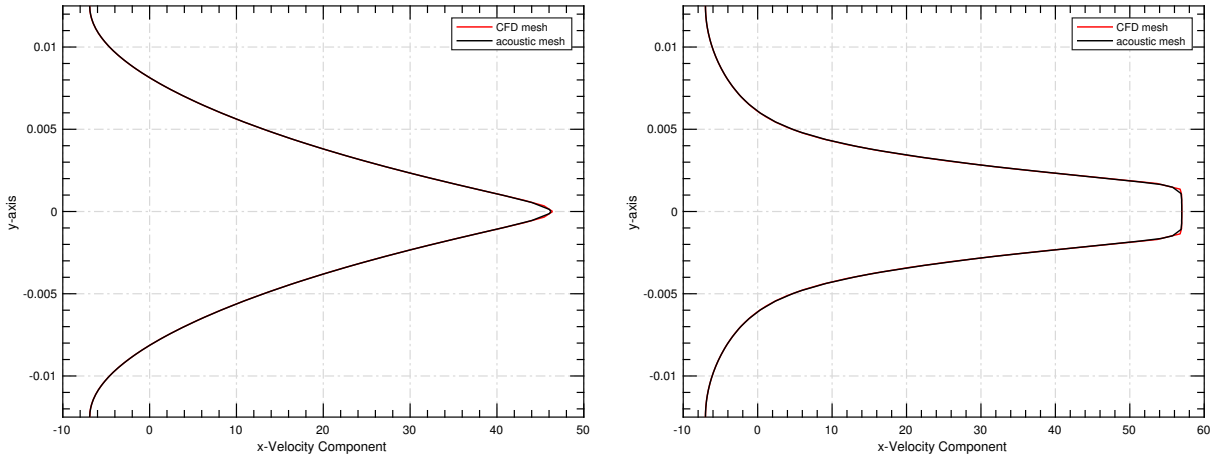

(a) at $x = 0.05\,\mathrm{m}$, located in the jet region.

(b) at $x = 0.15\,\mathrm{m}$, located in the donwstream channel flow.

Figure 5. Comparison of the velocity profile between the CFD mesh and the acoustic mesh.

5 ACOUSTIC SIMULATIONS

As the mean flow field is calculated already, the perturbed field including both acoustic as well as vorticity perturbations is solved through the Eqs. (1). The simulations are carried out in COMSOL MultiphysicsV5.3, which is a commercial finite element method (FEM) solver. The Mach number and the frequencies are chosen corresponding to those measured in the experiments of [1]. The frequency of the incident wave is 150 Hz, 250 Hz and 350 Hz, respectively. The seven mean flow velocities are: $\mathbf{u}_{in} = 5.0, 7.5, 9.5, 11.5, 13.5, 14.5$ and 15.5 m/s, corresponds to the Mach number: $Ma = 0.015, 0.021, 0.027, 0.033, 0.039, 0.042$ and 0.045.

As shown in Fig. (6) and Fig. (7), at the cylinders, acoustic waves are scattered, part of the acoustic waves are transmitted downstream and part of the acoustic waves are reflected upstream. Besides that, some of the acoustic energy is transferred to the vorticity waves. The vorticities are convected by the mean flow, those become even stronger in the shear layer of the flow.

In order to obtain the acoustic scattering properties for the heat exchangers with tube-row geometries, and to compare with experimental results, the perturbed field is decomposed into upstream and downstream propagating acoustic waves. The acoustic properties are then formulated as a scattering matrix by using the Two Microphone technique (TMM), more details about the TMM can be found in [2]. The magnitudes of the enthalpy scattering matrix calculated from simulations as well as experimental results are shown in Fig. (8). In the experiments, usually the acoustic pressure is measured, however, the enthalpy scattering matrix is present in this paper by using the convention below [1]:

$$\underbrace{\begin{bmatrix} T^P_{1\to 2} & R^P_2 \\ R^P_1 & T^P_{2\to 1} \end{bmatrix}}_{\text{Measurements}} = \underbrace{\begin{bmatrix} T_{1\to 2}\left(\frac{1+M_1}{1+M_2}\right) & R_2\left(\frac{1-M_2}{1+M_2}\right) \\ R_1\left(\frac{1+M_1}{1-M_1}\right) & T_{2\to 1}\left(\frac{1-M_2}{1-M_1}\right) \end{bmatrix}}_{\text{Scattering elements plotted in Fig. (8)}} \tag{5}$$

M_1 refers to the Mach number at the inlet of the duct, while, M_2 refers to the Mach number further downstream of the heat exchanger.

As can be seen from Fig. (8) the results from the simulations are in good agreement with the experimental results from [1]. The numerical results predict the scattering of enthalpy precisely when the incident wave is imposed from the downstream side, corresponding to the scattering matrix elements $|T_{2-1}|$ and $|R_2|$. There are

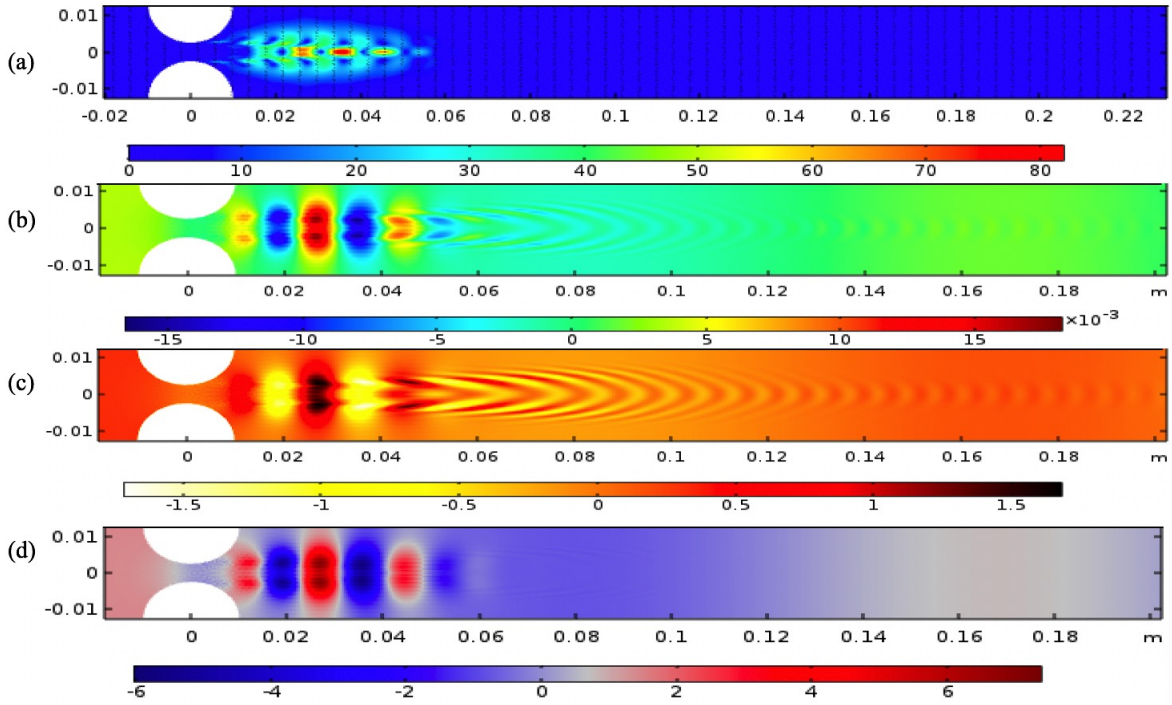

Figure 6. Perturbed field at frequency $f = 2000\,\mathrm{Hz}$ for $Ma = 0.033$ (a) particle velocity perturbations in [m/s] (b) density perturbations in [kg/m^3] (c) temperature perturbations in [K] (d) pressure perturbations in [Pa].

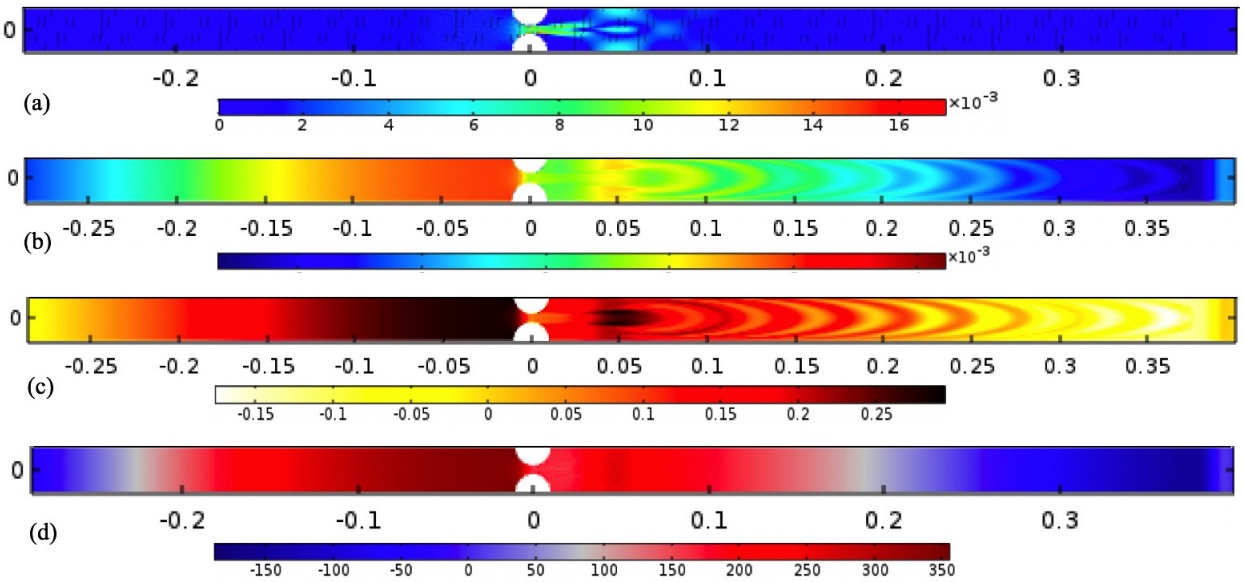

Figure 7. Perturbed field at frequency $f = 350\,\mathrm{Hz}$ for $Ma = 0.033$ (a) particle velocity perturbations in [m/s] (b) density perturbations in [kg/m^3] (c) temperature perturbations in [K] (d) pressure perturbations in [Pa].

more discrepancies for the scattering matrix element $|R_1|$ compared with the experimental results, and this is possibly due to inaccuracies in the simulations of the meanflow, i.e., the thickness of the shear layer or the reattachment point of the flow. It has been noticed that $|R_1|$ seems to be the scattering matrix element that is most sensitive to mean flow errors [3]. In the acoustic numerical simulations, it is always a difficulty to reproduce the same flow profile as the measurements.

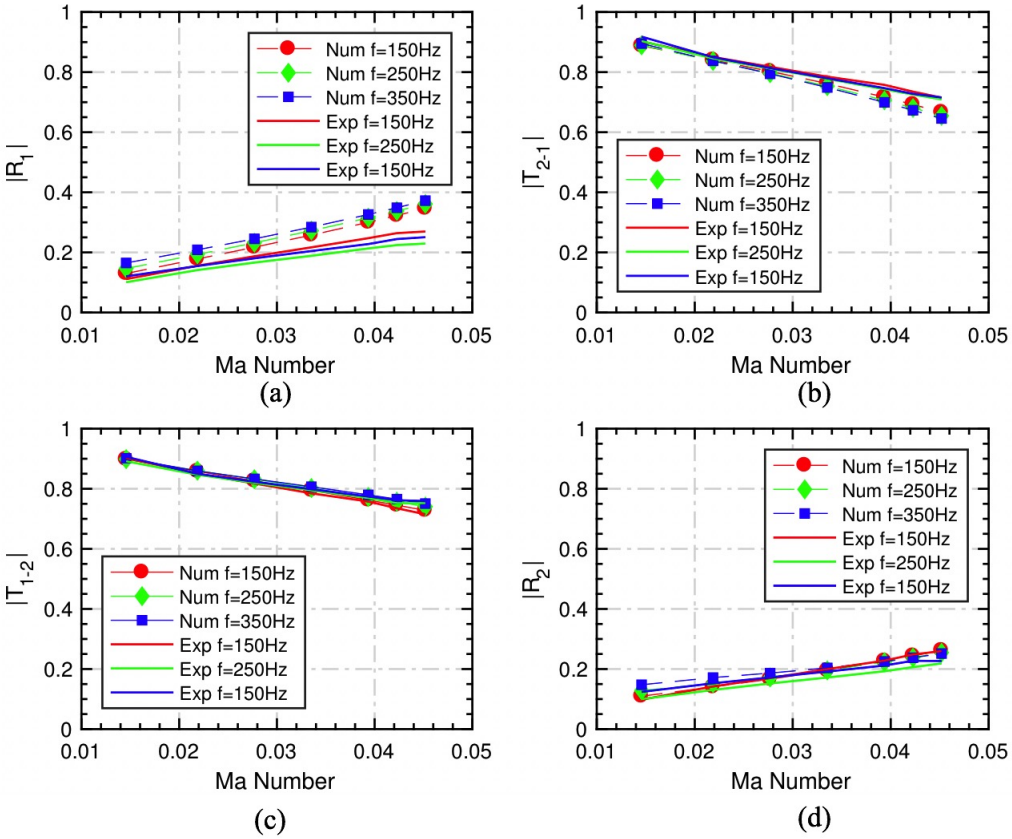

Figure 8. Magnitudes of the enthalpy scattering matrix, plotted as a function of Ma number at frequencies $f = 150, 250, 350$ Hz, respectively. Dashed lines with markers: simulations, solid lines: experimental results from [1].

6 CONCLUSIONS

In this paper, a numerical study of the acoustic scattering from tube-row heat exchangers with bias-flow at seven different Mach numbers is carried out. The simulations are performed by means of solving the linearized Navier-Stokes equations (LNSE) in frequency domain, taking into account the hydrodynamic effect as well as the viscous effect. The numerical methodology has been improved through solving the energy equation, instead of using the isentropic relation for the acoustic field compared with the previous work at KTH [4], [5], [6].

The numerical results presented in this paper clearly show that the sound-vortex interaction is resolved by the current numerical methodology, the sound vortex is generated along the shear layer of the jet flow and convected by the mean flow downstream of the heat exchangers, the energy is thus transferred from the hydrodynamic mode to the vorticity mode. In addition, the acoustic scattering matrix in terms of enthalpy is compared to the experimental results when bias-flow is present, and good agreement is found. It indicates that the flow

effects with the Mach number up to $Ma = 0.045$ are not negligible on the acoustic response in tube-row heat exchangers. For future work, the acoustic response with incident waves at higher frequencies will be examined and the heat transfer will be included in the heat exchanger simulations.

ACKNOWLEDGEMENTS

This research was financially supported by the Marcus Wallenberg Laboratory for Sound and Vibration Research (MWL) at KTH, Sweden.

REFERENCES

[1] Aswathy Surendran, Maria A Heckl, Luck Peerlings, Susann Boij, Hans Bodén, and Avraham Hirschberg. Aeroacoustic response of an array of tubes with and without bias-flow. *Journal of Sound and Vibration*, 434:1–16, 2018.

[2] Hans Bodén and Mats Åbom. Influence of errors on the two-microphone method for measuring acoustic properties in ducts. *The Journal of the Acoustical Society of America*, 79:541–549, 1986.

[3] Emma Alenius. CFD of duct acoustics for turbocharger applications. 2010.

[4] W. Na, G. Efraimsson, and S.Boij. Simulations of the scattering of sound waves at a sudden area expansion in a 3D duct. In *ICSV 21: The 21st International Congress on Sound and Vibration*, 2014.

[5] Wei Na. Frequency domain linearized navier-stokes equations methodology for aero-acoustic and thermoacoustic simulations. 2015.

[6] A. Kierkegaard, S. Allam, G. Efraimsson, and M. Åbom. Simulations of whistling and the whistling potentiality of an in-duct orifice with linear aeroacoustics. *Journal of Sound and Vibration*, 331:1084–1096, 2012.